Experimental and theoretical study of the erosion of semi-crystalline polymers and the subsequent generation of microparticles.

Thibaut Gaillard, Matthieu George, Emmanuelle Gastaldi, Frédéric Nallet, Pascale Fabre

Soft Matter

Accepted Manuscript

This article can be cited before page numbers have been issued, to do this please use: T. Gaillard, M. George, E. Gastaldi, F. Nallet and P. Fabre, *Soft Matter*, 2019, DOI: 10.1039/C9SM01482A.

ROYAL SOCIETY OF CHEMISTRY

rsc.li/soft-matter-journal

View Article Online
DOI: 10.1039/C9SM01482A

Journal Name

ARTICLE TYPE

Cite this: DOI: 00.0000/xxxxxxxxxx

Experimental and theoretical study of the erosion of semi-crystalline polymers and the subsequent generation of microparticles. †

Thibaut Gaillard,[a] Matthieu George,[a] Emmanuelle Gastaldi,[b] Frédéric Nallet,[c] and Pascale Fabre[a]

Received Date
Accepted Date

DOI: 00.0000/xxxxxxxxxx

The increase of plastics and microplastics in the environment is a major environmental challenge. Still, little is known about the degradation kinetics of macroplastics into smaller particles, under the joint actions of micro-organisms and physico-chemical factors, like UV or mechanical constraints. In order to gain insight into (bio)-degradation in various media, we perform accelerated erosion experiments by using a well-known enzymatic system. We show that the microstructure of semi-crystalline polymers plays a crucial role on the pattern formation at their surface. For the first time, the release of fragments of micrometric size is evidenced, through a mechanism that does not involve fracture propagation. A geometric erosion model allows to quantitatively understand erosion rates and surface patterns, and provides a critical heterogeneity size, parting two types of behavior: spherulites either released, or eroded *in situ*. This new geometric approach could constitute a useful tool to predict the erosion kinetics and micro-particles generation in various media.

1 Introduction

Pollution by plastic litter has become a major environmental problem resulting from their accumulation in terrestrial and marine environments. The fragmentation of plastics into microplastics is the most challenging issue[1–9]: in addition to the fact that microplastics are impossible to remove from the ocean, which is their ultimate receptacle, they are even more damaging than the macro waste. . Various studies have shown that microplastics are ingested by many types of marine organisms leading to adverse effects at several levels of the food chain and of the marine ecosystems[10–12]. It is also suspected that microplastics, that constitute a new habitat for micro-organisms, are vectors for potentially pathogenic bacteria[13–16].

It is well-known that the major fraction of ocean microplastics are secondary particles coming from the prior fragmentation of macroscopic waste during their use or after their disposal[17]. Therefore, the formation of polymer microparticles happens in a variety of media, from rivers to beaches, compost and soil. The fate of polymers in the environment depends on a number of factors whose relative importance varies according to the medium and stage of polymer degradation: abiotic phenomena (UV, mechanical stress), and biotic ones such as the colonization of plastics by micro-organisms (bacteria, phytoplankton, fungi, etc.)[18,19]. Abiotic phenomena are preponderant in media such as the water surface or beach zones[17], whereas biotic ones are likely to be the major degradation agents in soil or compost.

A primary step for bio-degradation is the constitution of a biofilm and a critical stage in the bio-degradation process is the deterioration of the polymer by exo-enzymes[20]. These enzymes are proteins secreted by cells, exhibiting a catalytic activity and involved in the breakdown of large macromolecules into oligomers small enough to go through cellular membranes for their assimilation. While abiotic phenomena lead to the damage and fragmentation of a polymer by oxidation and hydrolysis mechanisms, creation of structural defects and fracture propagation, it is generally considered that only biotic phenomena will result into the complete bio-degradation of a polymer, *i.e.* its conversion into biomass, water and CO_2. However, there is no certainty that a surface erosion mechanism such as the polymer degradation resulting from enzymatic hydrolysis won't lead also to fragment generation. The many studies done on bio-degradation of semi-crystalline polymers *via* bacteria colonization or enzymatic hydrolysis have evidenced the formation of surface erosion patterns[21–24] that sug-

[a] *Laboratoire Charles Coulomb (L2C), Université de Montpellier, CNRS, Montpellier, FRANCE*
[b] *Ingénierie des Agropolymères et Technologies Émergentes (IATE), INRA/ENSA.M/UMII/CIRAD, Université de Montpellier, Montpellier, FRANCE*
[c] *Univ. Bordeaux, CNRS, Centre de recherche Paul-Pascal, UMR 5031, F-33600 Pessac, FRANCE*

† Electronic Supplementary Information (ESI) available: [details of any supplementary information available should be included here]. See DOI: 00.0000/00000000.

View Article Online
DOI: 10.1039/C9SM01482A

gest the possibility of fragments release. When it comes to characterizing the erosion kinetics, though, studies often don't include the specificity of the erosion patterns observed[19,25,26] and the role of crystallinity is mostly interpreted in relation to the bulk polymer crystallinity and to average erosion rate differences between crystalline and amorphous (rigid or free) regions, which are due to differences in accessibility of their reactive groups for enzymatic hydrolysis[26–30].

Enzymatic degradation of polyesters, like polylactide (PLA) or Poly(3-hydroxybutyrate-co-3-hydroxyvalerate) (PHBV), which are good candidates for biodegradability, has been widely studied. PLA hydrolysis can be catalyzed by Proteinase K[31] and it has been shown that the main physico-chemical parameters affecting the polymer hydrolysis rate are molar mass[32], stereo-chemistry of L and D-mers[33–35] and crystallinity[26,34].

In this paper, we focus on quantitatively understanding how surface erosion proceeds in a semi-crystalline polymer. More specifically, we explore how the polymer micro-structure and heterogeneities at the microscale influence the erosion process and fragments generation. We use the well-known system PLA/Proteinase K as a general model of the erosion process of a semi-crystalline polymer. Using a polymer of a given chemical composition, we monitor its micro-structure at the micron scale through its crystallinity ratio, everything else remaining constant. Let us underline that the spherulite-type microstructures developed in PLA appear in almost all types of manufactured polymers[36], *e.g.* polystyrene (PS), polyethylene (PE). Moreover, the high hydrolysis rate of PLA by proteinase K allows to perform accelerated erosion experiments at the laboratory scale. The degradation patterns of the polymer are characterized in parallel with their erosion rates. The results are interpreted with a model that takes into account the geometry of crystalline regions and their evolution with the degradation time.

2 Materials and Methods

2.1 Preparation and characterization of PLA films

PLA pellets were purchased from Unitika Terramac Ltd, Japan. The polymer is a poly-DL-lactic acid that contains a small amount (1.7%) of D-mer, with a molecular weight $M_n = 95$ kg/mol and a polydispersity index $I = 1.63$, according to the supplier. This percentage of D-mer allows to prepare either amorphous or crystalline samples, depending on the processing parameters.

Pellets were hot embossed and degassed, then maintained in a hydraulic press at 180°C under a pressure of 7 bars during 9 minutes, and eventually quenched in a second press at 25°C to obtain amorphous samples. Films were then annealed at 110°C for 20 (SC5) or 110 minutes (SC35) under vacuum. The bulk crystallinity χ_b–averaged over their volume–for the three types of films, was measured by DSC and is reported in Table 1. Thermal analyses were carried out using a TA instrument DSC Q200 under nitrogen atmosphere. A thermal ramp of 5°C/min was used during the first run of heating and the second run of cooling with a temperature ranging from −40°C to 150°C and −40°C to 200°C, respectively. The crystallinity degree of samples was calculated from thermograms using equation $\chi_b = \Delta H_m / \Delta H_m^0$ where ΔH_m is the melting enthalpy and ΔH_m^0 the melting enthalpy of the polymer supposed to be 100% crystalline, *i.e.* $\Delta H_m^0 = 96$ J/g[37]. For all samples, $T_g = 60$°C and $T_f = 167$°C. Film thicknesses are ranging between 250 and 300 μm.

Since the knowledge of the overall crystallinity is not sufficient for our purpose, we also characterized the films micro-structures with polarized optical microscopy (POM), atomic force microscopy (AFM) and cross-section scanning electron microscopy (SEM). These experiments allowed us to precisely determine the samples micro-structures, which are sketched in Fig. 1. Both semi-crystalline samples exhibit a classical spherulitic structure, with smaller spherulites surrounded by amorphous polymer in SC5 and bigger spherulites that are in close contact for SC35. On top of this, a transcrystalline layer* is observed for both samples at the air interfaces.

Name	χ_b (%)	D_s (μm)
Amorphous (Am)	0.6 ±0.2	-
Semi-Crystalline (SC5)	5 ±0.5	10 ±5
Semi-Crystalline (SC35)	35 ±0.5	40 ±10

Table 1 Crystalline properties of PLA films. χ_b is the averaged crystallinity of the films as determined by DSC and D_s the mean characteristic diameter of the observed spherulites in the bulk material measured by POM.

2.2 Enzymatic erosion experiments

Proteinase K from *Tritirachium album Limber* (Sigma-Aldrich), an enzyme known to catalyze the hydrolytic degradation of ester groups[39,40], was used for the degradation of PLA. Experiments were performed in the following conditions: $T = 28$°C, immersed surface of PLA samples ~ 100 mm^2, pH = 8 (Tris-HCl buffer, concentration *ca.* 50 mM), NaN_3 as antibacterial agent. The enzyme concentration was $c_0 = 0.1$ mg/mL. The principle of the experiment is sketched in Fig. 2. Prior to the experiment, all films are systematically rinsed with ethanol and ultra-pure water, dried with nitrogen gas, and weighed. Each PLA film is then dipped into a 10 mL buffered solution of Proteinase K, and placed into the oven at temperature $T = 28$°C. After a given time, going from a few minutes to several days, films are withdrawn from the solution, dried at room temperature for a few minutes, and weighed again. After several days of drying at room temperature the surface topography is characterized by AFM and SEM. Reference samples were also immersed in sterile water at a temperature $T = 28$°C for 10000 minutes (one week). No alteration of the surface or weight loss were detected.

3 Results of the erosion experiments

For the sake of clarity in the following discussion, results will be presented according to the different types of microstructures observed in the samples regardless of their nominal crystallinity,

* Trans-crystalline layers are currently reported in semi-crystalline polymers[38] and can be due to thermal and/or hydrodynamic gradients at the interface with the mould pieces during polymer processing. The preparation method described above is consistent with such gradients.

View Article Online
DOI: 10.1039/C9SM01482A

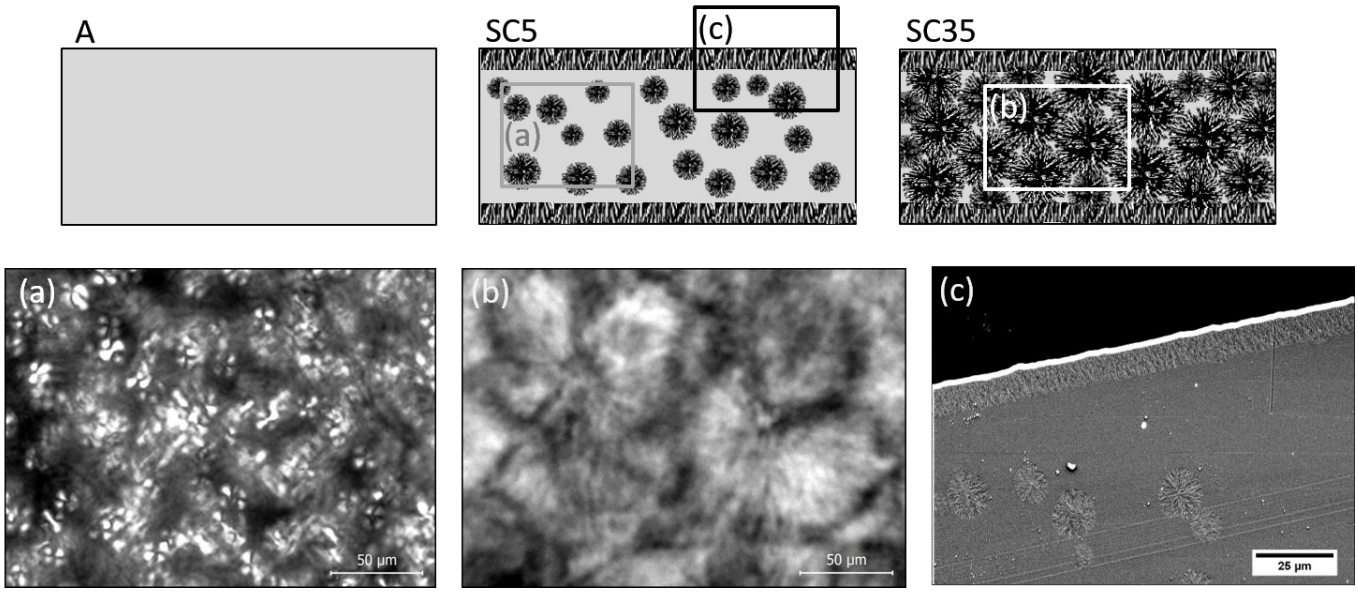

Fig. 1 Schematic microstructures of the three types of films: amorphous (A), semi-crystalline (SC5) and semi-crystalline (SC35) with respective overall crystallinities of 0, 5 and 35 % (side view). (a) and (b) POM images of the central part of respectively SC5 and SC35 samples (top view). (c) SEM cross section of the SC5 sample (side view). SC5 is constituted of spherulites embedded in an amorphous matrix (picture a), except for a transcrystalline layer at interfaces with air (picture c). SC35 is constituted of densely packed spherulites (picture b), except for a similar transcrystalline layer. Spherulites typical diameters D_s are reported in Table 1. The transcrystalline layer has a thickness of typically $\simeq 15\ \mu$m for both types of semi-crystalline films, and possibly a higher degree of crystallinity than the rest of the sample.

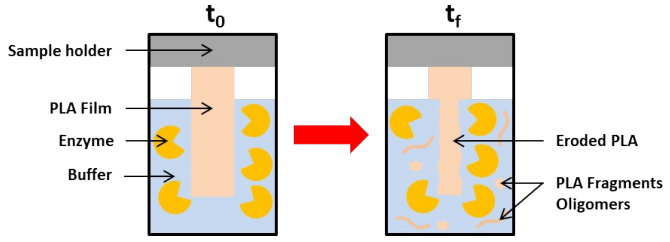

Fig. 2 Sketch of the enzymatic degradation setup, side view. Aspect ratio of the immersed part of PLA films typically $\sqrt{100}/0.3$, *i.e.* ≈ 30

namely: amorphous (Am), trans-crystalline (SC5 and SC35 surface layer), spherulitic phase (dense spherulitic for SC35 bulk or spherulites dispersed in amorphous phase for SC5 bulk). Patterns formation will be described for each microstructure, then weight loss curves will be displayed for all samples.

3.1 Erosion pattern for the amorphous morphology

In Fig. 3, one observes using AFM that the erosion of amorphous regions is not completely homogeneous, but proceeds through the opening of craters that most probably initiate at defects (small bubbles, impurities). These craters are very flat (average depth 0.3 μm for an average radius of 1 μm) and they become larger and more numerous until they collide, thus increasing the RMS roughness on $40 \times 40 \mu m^2$ areas from 35 nm to 130 nm.

3.2 Erosion pattern for the trans-crystalline microstructure

From SEM images (Fig. 4), one can observe that the trends followed by SC5 and SC35 in terms of erosion patterns are very similar. In both cases, anisotropic holes open inside non- or less-eroded regions leading to the progressive formation of a porous-type layer at the sample surface. The characteristic dimension of the final pores is of the same order of magnitude in SC5 and in SC 35 ($\simeq 700$ nm). These results can be explained by the similar morphology of the trans-crystalline layer in both SC films. The holes anisotropy is probably due to local flows happening during polymers processing.

3.3 Erosion pattern for the spherulitic microstructures

In bulk, SC5 is composed of spherulites of sizes of the order 10 μm, embedded in an amorphous phase whereas in SC35, these spherulites have grown to reach a typical size of the order 40 μm at which they are densely packed. SEM observations performed on the lateral sides of the polymer films allowed to observe the erosion evolution of these two morphologies. In Fig. 5, for polymer SC5, one can clearly see a spherulite about to detach from the bulk, since the surrounding amorphous phase was almost totally eroded. The spherulite itself was eroded faster in its amorphous regions than its crystalline ones, leading to this 'morel-type' appearance. The erosion patterns of the lateral sides of SC35 films are completely different (Fig. 5). One does not observe a series of packed convex (emerging) eroded spherulites as one could have extrapolated from SC5 behavior, but rather, concave eroded zones that could be interpreted as *in situ* eroded spherulites, mixed with disorganized eroded regions. At that stage, one can not conclude on the origin of this behavior difference between SC5 and SC35. However, it is worth noting one extra fact from Fig. 5 (left): the big background spherulite, still half embedded in the amorphous phase, is truncated at its top, therefore also displaying a concave

View Article Online
DOI: 10.1039/C9SM01482A

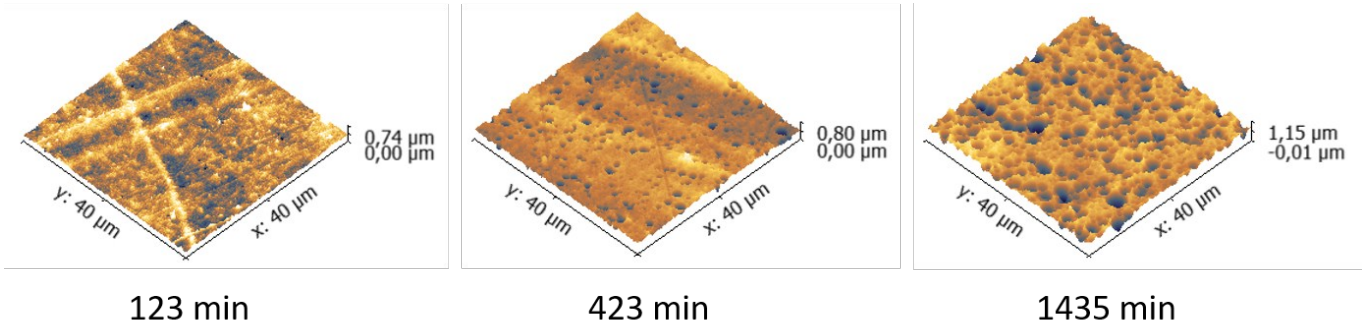

Fig. 3 Evolution of the eroded surface of the amorphous PLA observed by AFM after respectively 123, 423 and 1435 minutes: 3D representation of the topography.

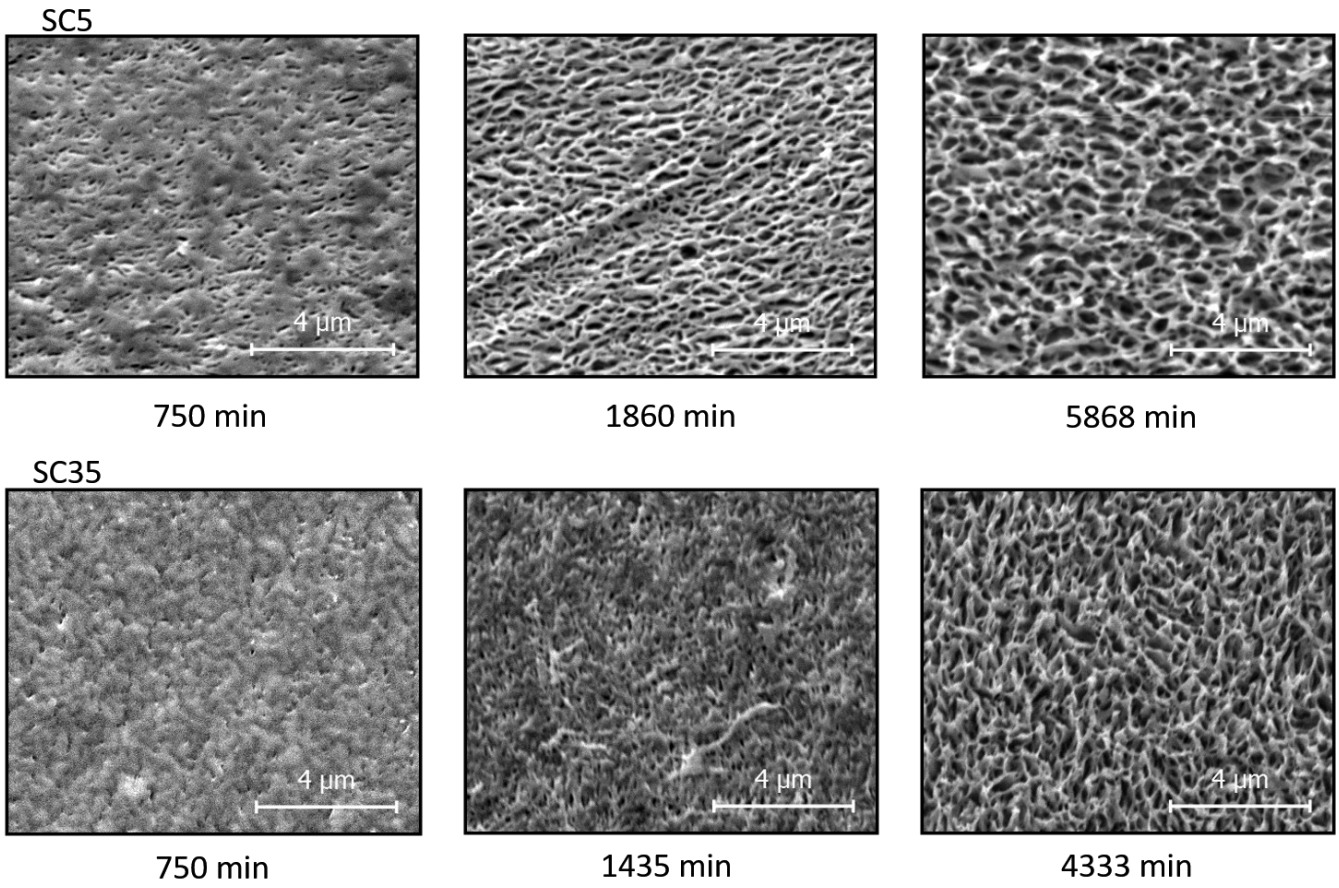

Fig. 4 Evolution of the eroded surface of SC5 (upper row) and SC35 (lower row) observed by SEM after respectively 750, ≃1500 and ≃5000 minutes. Top views

View Article Online
DOI: 10.1039/C9SM01482A

shape.

3.4 Weight loss curves

The evolution of the weight loss Δm (normalized by the immersed sample surface S) *versus* time is shown in Fig. 6 for all samples. The weight loss curves are not linear but display a slowing down with long degradation times, particularly visible for the amorphous sample. Through measuring the enzymatic activity by classical azocasein spectrophotometric assay[41] over the same time duration as our degradation experiments, we checked that this deviation from a linear behavior *cannot* be attributed to a decrease in the enzymatic activity. In semi-crystalline samples, whereas the slowing-down trend is similar to amorphous samples, the initial weight loss rate is all the lower as the nominal crystallinity is high. This is a classical result since the crystalline erosion rate is much smaller than the amorphous one[29]. Most authors use a linear effective medium approximation to quantitatively interpret the initial erosion rates as a function of the crystalline ratio[26]. In our case, the crystalline ratio of the transcrystalline layer, where the erosion takes place, is *a priori* different from the bulk crystallinity as determined by DSC (Table 1) and therefore not known. In order to discuss further the specific trends of these curves (slope at origin, characteristic slowing-down time) we first will develop, next section, a model of surface erosion, driven by enzymatic degradation. Quantitative comparison between these curves and the model will be achieved later, in a specific section.

4 Two phases geometric erosion model (GEM)

Numerous analytical or numerical models have attempted to predict the kinetics of enzymatic degradation[19,42–46]. These models are difficult to compare since they rely on very different assumptions. Moreover, as stated by Laycock in a recent review[19]: "there is no general model developed to date that adequately describes in full the progress of enzymatic degradation of biodegradable polymers, taking into account the heterogeneity of the system". In semi-crystalline polymers, enzymatic degradation is selective and driven by the material structure at the micron scale. The key feature of the present approach is to consider the heterogeneity of the material at that scale and its impact on the surface roughness and on the erosion rate. The phenomenological geometric model proposed here, based on periodically alternating amorphous and crystalline regions, allows to interpret both the observed (surface) erosion patterns and weight loss experiments.

In a semi-crystalline material, it is easy to understand that the coexistence of a quickly degrading (amorphous) phase and a slowly degrading (crystalline) phase will lead to the increase with time of the surface exposed to erosion for the slower degrading material (here crystalline), thereby somehow blurring the distinction between surface and bulk erosion, as already demonstrated in early numerical simulations[47]. The patterning that appears during the enzymatic and bacterial erosion of many semi-crystalline bio-degradable polymers [21–24] is a consequence of this point. In this section, we examine a crucial and often overlooked consequence of this surface increase–namely the evolution of the erosion rate and erosion front with time–through a two phases geometric erosion model (GEM).

For the sake of simplicity, the sample is represented as a one-dimensional, periodic stack (period λ) of amorphous and crystalline layers. A cut of such a bulk structure along a plane containing the stacking axis appears as a periodic flat surface, with alternating amorphous and crystalline strips with the same period λ (see Fig. 7). At time 0, the surface is exposed to the enzymatic solution and erosion starts. We assume that it proceeds *normally* to the (local) surface tangent plane. The erosion rate $e(t)$, which is the derivative of the weight loss over time, can be expressed for each phase as:

$$e(t) = \frac{d\Delta m}{dt} = \rho S_e(t) v \tag{1}$$

where ρ is the mass density, v the erosion front velocity and $S_e(t)$ the (actually *time-dependent*) surface exposed to the eroding solution.

Two phases only are considered in the model, namely amorphous and crystalline, neglecting the existence of free amorphous and rigid amorphous phases[26]. All transport phenomena are assumed to occur instantaneously. In the amorphous regions (Am in white), the surface remains flat and the erosion front moves perpendicularly to the surface *i.e.* vertically with velocity v_a. In the crystalline regions (Cr in grey), the erosion front also moves perpendicularly to the (initially horizontal) surface, but with a smaller velocity v_c, which implies that the *orientation* of the erosion front may change locally. During a time interval δt, point B will move perpendicular to the surface by an amount $v_a \delta t$ while point A will move in both horizontal and vertical directions with parallel and perpendicular velocities such that the slanted AB plane moves by a distance $v_c \delta t$, while keeping a constant orientation. As a consequence, extra crystalline surface is gradually created and exposed to enzymatic degradation. If the velocity ratio v_c/v_a always keeps a constant value, the AB portion of this crystal surface will be eroded while staying parallel to itself, with an angle α with respect to the (initial) normal to the surface:

$$\sin\alpha = \frac{v_c}{v_a} \tag{2}$$

Lateral erosion continues until point A reaches its counterpart at a time t_c, when the horizontal crystalline mesa disappears, that can be calculated with elementary geometry to be solution of the equation:

$$\frac{\chi\lambda}{2} = \tan\alpha \int_0^{t_c} (v_a - v_c) du \tag{3}$$

which becomes explicit in the case where the two erosion velocities are constant:

$$t_c = \frac{\chi\lambda}{2\tan\alpha(v_a - v_c)} \approx \frac{\chi\lambda}{2v_c} \tag{4}$$

where the rightmost side of eq. (4) holds in the limit $v_c \ll v_a$. At times larger than t_c, the surface shape does not evolve any more, and the spike-shaped erosion front moves as a whole with the 'amorphous' velocity v_a. This can be explained with a simple

View Article Online
DOI: 10.1039/C9SM01482A

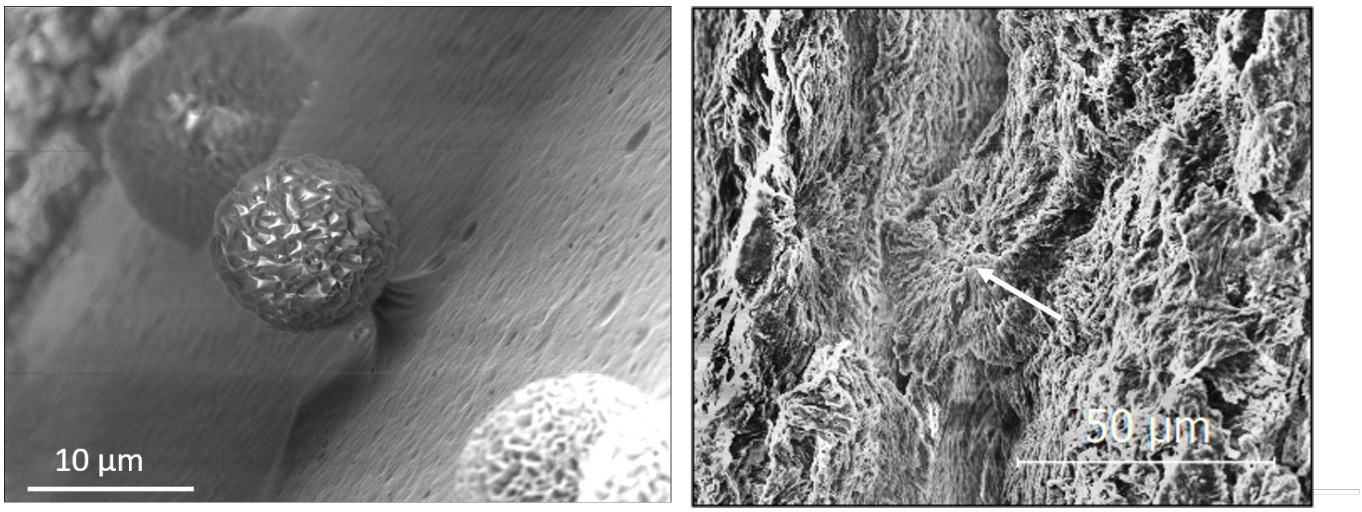

Fig. 5 SEM observation at t ≃ 8000 min for the erosion of (left) small spherulites embedded in amorphous phase (SC5) (right) dense spherulitic phase (SC35). These two pictures were acquired on the lateral side of the polymer films. On the right image, an arrow indicates the centre of an *in situ* eroded spherulite

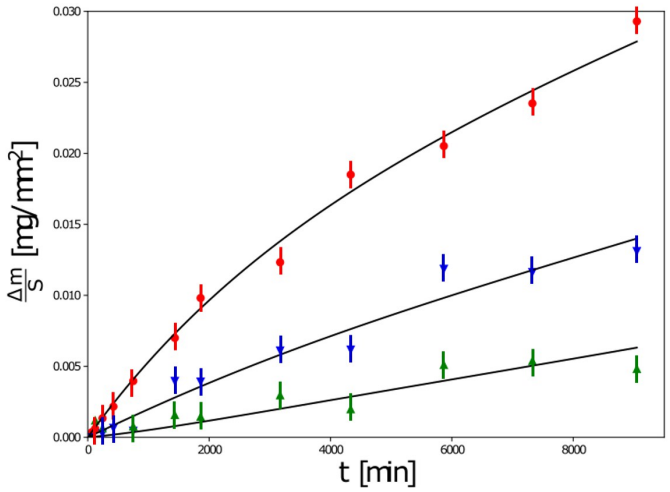

Fig. 6 Evolution with time of the weight loss per surface unit for amorphous (red circles), SC5 (blue inverted triangles) and SC35 (green triangles) samples. Continuous black lines: best fits to experiments – see text for model details.

hand-waving argument: the stationary shape corresponds to an amount of material removed from the surface in the crystalline region which is exactly equivalent to what would be removed from an amorphous region that has the same projected area.

Therefore, two regimes are expected for the erosion of a semi-crystalline polymer and the erosion per unit *initial* area S can be expressed as:

$$\text{for } t < t_c,\ \frac{d\Delta m}{dt} = \rho S\left[(1-\chi)v_a + \chi v_c + 2\tan\alpha\,\frac{v_a - v_c}{\lambda}\int_0^t (v_a - v_c)du\right] \quad (5)$$

$$= \rho S\left[(1-\chi)v_a + \chi v_c + \chi(v_a - v_c)\frac{t}{t_c}\right] \quad (6)$$

$$\text{for } t \geq t_c,\ \frac{d\Delta m}{dt} = \rho S v_a \quad (7)$$

where the second line in the above expressions, eq. (6), is the simplified form of eq. (5) when erosion velocities v_a and v_c do not depend on time, and with ρ the polymer mass density (assumed to be identical for amorphous and crystalline phases for the sake of simplicity).

As represented in Fig. 8 when assuming constant velocities, for t smaller than the critical time t_c, the erosion rate of a semi-crystalline sample increases with time and its weight loss is all the smaller as its crystallinity is high. After this transient regime, the erosion rate reaches a constant value equal to the erosion rate of the amorphous phase. The reason why semi-crystalline materials are generally thought of as eroding slower than amorphous ones is mostly due to their *initially* lower weight loss rate. After this initial lag time, the model shows that the weight loss accelerates and the erosion finally proceeds at the same velocity in a semi crystalline material or in an amorphous one. The larger the crystalline ratio, the smaller the initial erosion rate and the larger the characteristic time t_c, therefore the longer it takes to reach the same erosion rate as an amorphous material. An increase in the characteristic size λ of the microstructure will also increase the

View Article Online
DOI: 10.1039/C9SM01482A

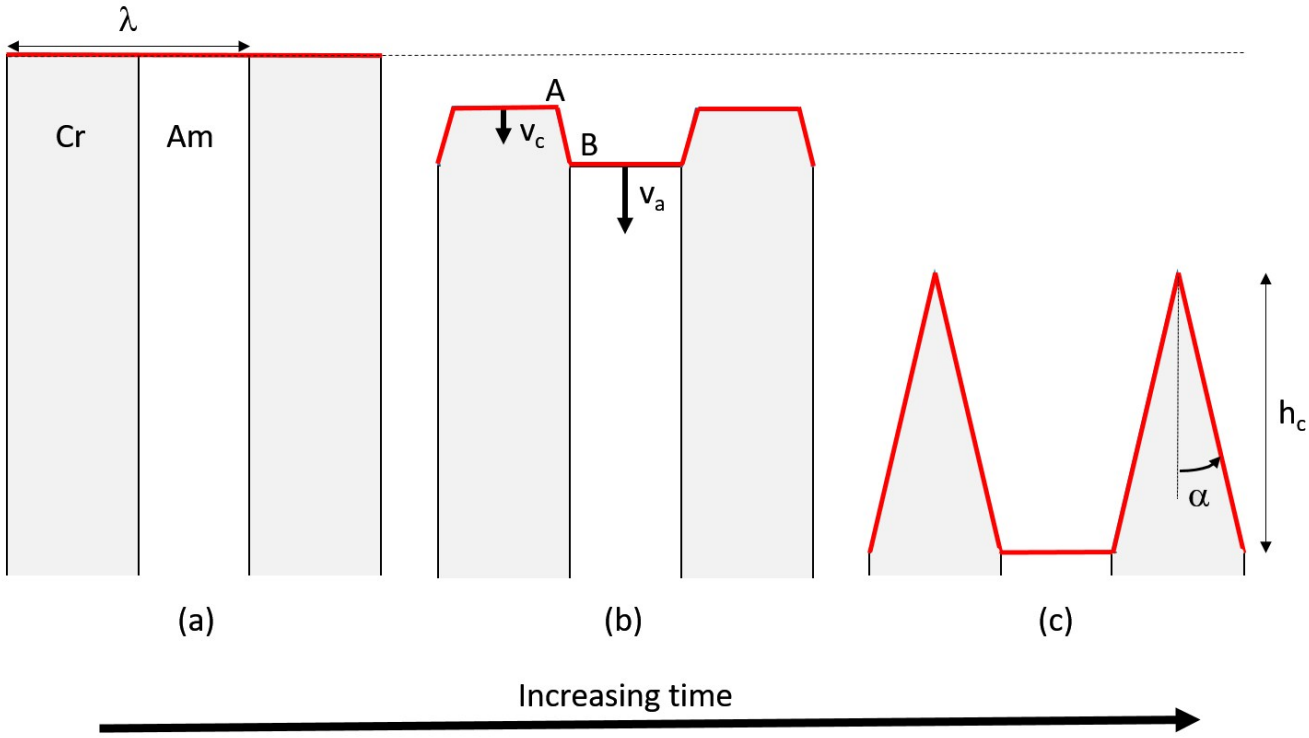

Fig. 7 Schematic of the geometric model at different erosion times. Initially flat (a) with alternating amorphous (Am in white) and crystalline (Cr in grey) regions, the surface gradually becomes rough with crystalline regions sticking out. After a transient regime (b), a stationary, spike-shaped surface is reached (c), and the whole surface is then eroded with a constant (effective) velocity equal to v_a. The erosion front is indicated in red.

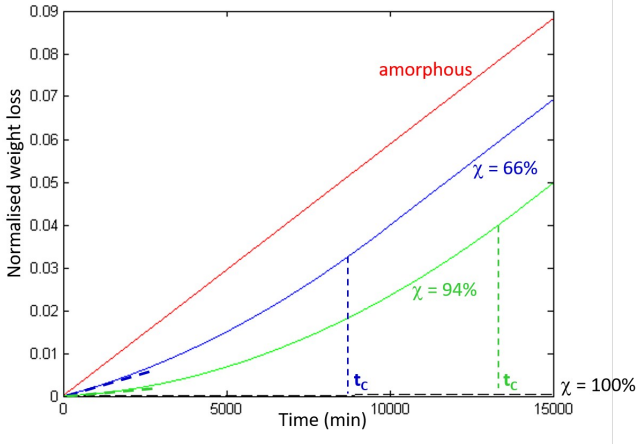

Fig. 8 Theoretical weight loss curves as a function of time for constant velocities, $v_a = 4.7$ nm/min and $v_c = 0.023$ nm/min, and $\lambda = 700$ nm. The four curves correspond to different crystalline ratios, which have been chosen to represent the respective crystalline ratio of the three samples Am, SC5 and SC35, as estimated from the fitting model (Table 2) and a theoretical wholly crystalline sample.

characteristic time t_c, meaning that the local structure of alternating amorphous and crystalline regions will affect the erosion rate. It is thus interesting to point out that to consider only the overall material crystallinity for discussing semi-crystalline polymers erosion front velocity is not sufficient.

The GEM description of the erosion process leads to new and counter-intuitive outcomes: it is shown that after a transient regime where the polymer surface is eroded and becomes rougher, not only does it keep the same shape while being eroded further, but the overall erosion rate is equal to the erosion rate of the amorphous phase and is independent of the material crystalline ratio χ. Important consequences of this behavior on the fragmentation of semi-crystalline polymers will be drawn in the last section.

5 Comparison between experimental results and GEM

In order to go further with the interpretation of the results, one more element needs to be considered. Indeed, assuming a *constant* erosion velocity is clearly *not* in agreement with the weight loss curves (Fig. 6), even in the simple case of a wholly amorphous system. In this section, we will therefore in a first step propose an interpretation for the decrease with time of the amorphous phase erosion rate. In a second step, considering non constant erosion front velocities in the geometric erosion model–in particular, following eq. (5)–will allow us to quantitatively compare the weight loss measurements to the proposed model.

View Article Online
DOI: 10.1039/C9SM01482A

5.1 Slowing-down of the erosion for an amorphous polymer in an enzymatic solution

The rate of erosion is dependent on the kinetics of the enzymatic hydrolysis reactions at the polymer surface. At the beginning of the experiment, we are in a situation where enzymes are in large excess which leads to a complete polymer surface coverage [48] and a high erosion rate. When more and more polymer chains are cut and released in solution, extra hydrolysis reactions take place in solution between released oligomers and enzymes, modifying the previous equilibrium and decreasing the polymer surface coverage by enzymes. The polymer erosion rate therefore decreases with a characteristic time depending on the kinetics of the different chemical reactions at play. A stationary state (constant erosion rate) is reached when the rate of oligomers release due to polymer surface erosion is equal to their hydrolysis rate in solution (this is based on the assumption that the surface adsorption equilibrium is instantaneously reached).

The previous mechanism accounts for a decrease of the erosion rate towards a constant non-zero value and it is therefore meaningful to adjust the experimental curve using three parameters–the initial and final erosion front velocities, resp. v_0 and v_∞, and a characteristic crossover time t_S–with the following equation:

$$v_a = (v_0 - v_\infty)e^{-\frac{t}{t_s}} + v_\infty \tag{8}$$

This interpretation is supported by numerical estimations of the enzyme concentration at the beginning and at the end of the experiment. From the total weight loss at the end of the experiment, one can estimate that 10^{16} polymer chains in total have been released in solution. At the same time, experiments show that the erosion rate v_∞ equals 1/3 of v_0. Following the results of Yamashita et al. [48], which established the relation between enzyme concentration and erosion rate in experimental conditions similar to ours, one can estimate a final enzyme concentration in our experiment $c = c_0/4$, corresponding to a decrease in the number of enzymes available at the surface, by an amount of 10^{16}. Even though many assumptions underlie the comparison between these two numbers (*e.g.* that chains are released in solution as soon as they are cut once, that there is one enzyme per chain in solution, ...), the fact that, at the end of the experiment, the number of enzymes occupied in solution is of the same order of magnitude as the number of released chains, is a good indicator that the explanation for the erosion slowing-down is compatible with our experimental conditions.

5.2 Geometric Erosion Model for non constant erosion front velocities and comparison to the experimental results

In order to fit the experimental weight loss curves obtained for all samples, we will now take into account the variation of the erosion front velocities with time. Let us notice that while eq. (5) is valid for non constant velocities $v_a(t)$ and $v_c(t)$, eq. (6) is not. In eq. (5), we therefore need to simply use eq. (8) for $v_a(t)$. Moreover, since the slowing-down mechanism is based on a depletion of the enzymes from the surface, it is reasonable to assume that v_c follows the same trend as v_a: $v_c(t) = \sin\alpha\, v_a(t)$ with a *constant* angle α. Performing the integration of eq. (5), one obtains:

$$\begin{aligned}\frac{\Delta m}{\rho S} &= [(1-\chi)+\chi\sin\alpha]\left[t_s(v_0-v_\infty)\left(1-e^{-\frac{t}{t_s}}\right)+v_\infty t\right] \\ &+2\tan\alpha\frac{(1-\sin\alpha)^2}{\lambda}\left[t_s^2(v_0-v_\infty)^2\left(1-e^{-\frac{t}{t_s}}\right)\right. \\ &-\frac{t_s^2}{2}(v_0-v_\infty)^2\left(1-e^{-\frac{2t}{t_s}}\right)+v_\infty(v_0-v_\infty)tt_s\left(1-e^{-\frac{t}{t_s}}\right) \\ &\left.+v_\infty^2\frac{t^2}{2}\right]\end{aligned} \tag{9}$$

when $t \le t_c$ and, integrating eq. (7):

$$\frac{\Delta m}{\rho S} = \left[t_s(v_0-v_\infty)\left(e^{-\frac{t_c}{t_s}}-e^{-\frac{t}{t_s}}\right)+v_\infty(t-t_c)\right]+\frac{\Delta m(t_c)}{\rho S} \tag{10}$$

in the long-time limit where $t > t_c$.

Note that eq. (3), which determines the characteristic time t_c for the end of the transient regime and the beginning of the stationary one–as far as building a spike-shaped surface is concerned–, remains an implicit equation:

$$\frac{\chi\lambda}{2} = \tan\alpha(1-\sin\alpha)\left[t_s(v_0-v_\infty)\left(1-e^{-\frac{t_c}{t_s}}\right)+v_\infty t_c\right] \tag{11}$$

Equations (9) and (10) describe the behavior of all three samples–namely amorphous, SC5 and SC35–, with six parameters, quite a huge number compared to the available data size. However, by construction, four of these parameters are the same for the three samples: v_0, v_∞, t_s and $\sin\alpha$, such that $v_c(t) = \sin\alpha\, v_a(t)$. Moreover, one can further constrain the fit by making reasonable assumptions and set certain parameters to experimentally sound values. First, λ should be similar for SC5 and SC35, since it is mostly determined by the intrinsic properties of the polymers and will essentially not vary with the annealing time. From SEM observations, one can estimate a reasonable value of $\lambda = 700$ nm for both samples. Finally, the ratio $\sin\alpha = v_c(t)/v_a(t)$ is taken from literature [26] and set equal to $1/200$. With these conditions, the three weight loss curves were fitted simultaneously. The agreement appears qualitatively quite good (cf. Fig. 6) and the fitting parameters are reported in Table 2.

v_0 (nm/min)	v_∞ (nm/min)	t_s (min)	χ_{SC5} (%)	χ_{SC35} (%)
4.7	1.4	3150	66	94

Table 2 Fitting parameters of the weight loss curves.
v_0 and v_∞ are respectively the initial and the final velocity of the erosion front in the amorphous phase, t_s is the characteristic time of the slowdown, χ_{SC5} and χ_{SC35} are the respective crystallinity of the transcrystalline layer in SC5 and SC35 samples

In order to check the self-consistency of the whole interpretation, it is interesting to discuss the values obtained from the fit by comparison either to literature or to more data coming from the present experiments.

Firstly, the value $v_0 = 4.7$ nm/min for the initial amorphous erosion rate is reasonably close to what is reported in literature for

View Article Online
DOI: 10.1039/C9SM01482A

PLA, $v_0 = 5.6$ nm/min[48], even though an exact comparison is not possible due to differences in parameters from one experiment to another (temperature, molar mass, stereo-chemistry). Regarding the initial erosion front velocity in the crystalline phase $v_c(0)$, on the one hand, it can be deduced from v_0 that $v_c(0) = 4.7/200 = 0.023$ nm/min. On the other hand, from SEM experiments, one can extract a value for $v_c(0)$, since it corresponds to the initial opening velocity of the holes, of around 0.03 nm/min, in quite good agreement with the value coming from the fit. Regarding the crystalline ratio χ, it is equal, respectively, to 66% and 94% for SC5 and SC35. As could be expected, the surface transcrystalline layer has an enhanced crystallinity compared to the bulk one[38]. Also, the larger crystallinity for SC35 compared to SC5 is consistent with a longer annealing time. The height h_c of the patterned layer forming the stationary front can be expressed as:

$$h_c = \frac{\chi\lambda}{2\tan\alpha} \tag{12}$$

From the fitting parameters, h_c is of the order of 10 μm for both semi-crystalline samples, *i.e.* slightly smaller than the thickness of the transcrystalline layer which is estimated to be 15 μm. Therefore this layer is not totally eroded during the complete duration of our experiment.

Finally, the critical times to reach the stationary GEM regime, when the surface shape of the material won't evolve anymore and the overall erosion rate of the crystalline material will be equal to the amorphous erosion rate, can be extracted from the fit. They are equal to $t_c \simeq 26000$ min (nearly 3 weeks) for SC5 and $t_c \simeq 40000$ min (about one month) for SC35. This is consistent with the fact that, in the time course of the experiments, we have not reached the stationary regime and the final stationary spike-shape surface yet. These results also mean that, in conditions where there is an excess of enzymes (at least at the beginning of the erosion), the equilibrium shape of PLA can be reached at 28°C within a few weeks only. From that point, even though it is still semi-crystalline, PLA will start eroding faster, with the amorphous erosion rate. These times have been obtained in model conditions in laboratory, and certainly suffer a large uncertainty, they nevertheless represent the first step towards a quantitative evaluation of a characteristic bio-degradation time for a material.

Insofar as GEM is an over simplified description of the erosion process in semi-crystalline samples, the comparison with experimental results seems quite satisfactory. Since the present data does not extend to large times, further validation of the model would imply experiments on longer time-scales, which are delicate to realize with stable enzymatic conditions.

6 Application to the potential release of microparticles

In the following, we use the model to describe spherulites erosion and to interpret some more features of the present experiments. As already mentioned, observations performed by SEM on the eroded lateral sides of SC5 and SC35 films (Fig. 5) display two different behaviors: either spherulites on the verge of being released or *in situ* eroded spherulites. By comparing the relative characteristic time t_{release} to release a spherulite of size D from the matrix to the characteristic time t_c needed to build the porous structure in the spherulite (see eq. 3) and reach the amorphous erosion rate, one can express the critical size D_c which draws the limit between objects released before being eroded and objects eroded *in situ*. One can assume that a spherulite will detach from the matrix when the erosion front of the amorphous phase has moved over a distance equal to its diameter D, *i.e.*:

$$t_{\text{release}} = \frac{D}{v_a} \tag{13}$$

where v_a is the erosion front velocity for the amorphous phase, assumed to be constant. Solving $t_{\text{release}} = t_c$, one can write:

$$D_c = \frac{v_a\lambda\chi}{2v_c} \tag{14}$$

Using typical values for a polymer[49], with spherulite characteristics of $\chi \simeq 50\%$, $\lambda \simeq 100$ nm and $v_a/v_c = 200$, one gets a critical size of the order of $D_c \simeq 5$ μm. Because this critical diameter is of the same order as a typical spherulite size, the two distinct behaviors–release or *in situ* erosion–are likely to be observed for usual polymers, in the same way as they seem to be observed here. This mechanism probably remains valid for materials constituted of densely packed spherulites, since the very thin layer of amorphous phase surrounding them will be eroded at least at the same rate as their inner amorphous part. The previous analysis could be applied to many materials, since most of them possess microstructure heterogeneities of typical sizes one to hundred microns. In this case, small spherulites might be systematically released and generate microparticles , while bigger ones might be eroded *in situ*, thus maintaining the integrity of the material.

7 Conclusions and Outlook

The strength of the GEM description developed in this article lies in the simplicity of its main ingredients – two phases eroding at a different rate and a surface only erosion mechanism – and therefore in its potential extension to other degradation processes. It allows to highlight and quantify, at least to the first order, the fundamental effect of material heterogeneity at a microscopic scale in the erosion process. Four major learnings can be inferred from the present model:

1. After a lag time related to its crystallinity and microstructure characteristic size, a spherulitic semi-crystalline polymer will be eroded, under the action of enzymes or micro-organisms, at the same rate as if it were amorphous.

2. During the erosion process, a spherulitic semi-crystalline polymer will roughen and develop a porous-like surface layer with typical dimensions of the order of a few microns. This roughness depends on the material characteristics and is quantified by the model. Such a roughening has already been observed on many plastic debris collected from the ocean[13,50]. This increase of surface roughness will play on contaminants adsorption, colonization by micro-organisms and fracture propagation.

View Article Online
DOI: 10.1039/C9SM01482A

3. A spherulitic semi-crystalline macroplastic submitted to surface erosion will potentially release hard structures of small size (typically $D < 10\mu$m) . These particles would probably have an eroded surface similar to what is observed in the present experiments (Fig. 5) (*e.g.* porous like or at least extremely rough).

4. The polymer microstructure plays a crucial role in the erosion process and the potential release of microparticles. Our model should apply to all semi-crystalline polymers exhibiting spherulites, which is the most common case. Salomez *et al*[51] have recently shown that in the case of micro-organisms degradation in compost, significantly different erosion patterns occur for polymers with different microstructures. It would be of great interest to study other types of microstructures and adjust the model to other topologies (for instance by using a different geometry for the periodic structure). One could extrapolate from the present approach that the larger the scale and the more inter-connected the microstructure of the semi-crystalline polymer, the less it is prone to release particles. Particles release from a biodegradable or non-biodegradable polymer could be monitored not only by playing on the chemistry and the stereochemistry of the material, but also by tuning its microstructure.

Whereas degradation is considered in general either at the molecular scale (macromolecules scissions and release of oligomers) or at the mesoscopic scale (fragmentation through mechanical weakening and fracture propagation), the approach proposed here focuses on the polymer microstructure – typically a few microns – and takes into account for the first time the impact of surface roughening. The present model is generic enough to describe other degradation mechanisms, as long as they are sensitive to the polymer microstructure and to the amount of exposed surface. For instance, by taking into account additional phenomena like diffusion of the reactive species, the model could be applied to hydrolysis or enzyme-mediated microorganism degradation. It is certainly an interesting field to explore in the future.
In the actual state of knowledge, it is challenging to quantify the relative importance of this erosion and particles generation mechanism, that does not involve any fracture, with respect to mechanisms such as *e.g.* the fragmentation occurring with photo-degradation. Nevertheless, since the kinetics of degradation strongly depends on the environmental conditions (compost, soil, rivers, ocean) and on the nature of the polymer litter, it is probably important to keep this mechanism in mind to better evaluate the end of life of polymers in general and biodegradable/recyclable polymers in particular.

Conflicts of interest

There are no conflicts to declare.

Acknowledgements

This project was supported by the LabEx NUMEV (2011-LABX-076) integrated into the I-Site MUSE. The authors thank Rosica Mincheva, Jean-Marie Raquez and Philippe Dubois for preparing the PLA samples and performing DSC characterisations. They acknowledge as well fruitful scientific discussions with Jean-François Ghiglione.

Notes and references

1 *Eunomia Reports*, June 2016.
2 D. Barnes, F. Galgani, R. Thompson and M. Barlaz, *Phil. Trans. R. Soc. B*, 2009, **364**, 1985.
3 A. Cózar, M. Sanz-Martin, E. Marti, J. González-Gordillo, U. B. and J. Gálvez, *PLoS ONE*, 2015, **10**, e121762.
4 K. Law, S. Morét-Ferguson, D. Goodwin, E. Zettler, E. DeForce and T. Kukulka, *Environ Sci Technol*, 2014, **48**, 4732–4738.
5 M. Eriksen, L. Lebreton, H. Carson, M. Thiel, M. CJ. and J. Borrero, *PLoS ONE*, 2014, **9**, e11913.
6 A. Cózar, F. Echevarría, J. I. González-Gordillo, X. Irigoien, B. Úbeda, S. Hernández-León, Á. T. Palma, S. Navarro, J. García-de Lomas and A. Ruiz, *Proceedings of the National Academy of Sciences*, 2014, **111**, 10239–10244.
7 J. Gigault, B. Pedrono, B. Maxit and A. Ter Halle, *Environmental Science: Nano*, 2016, **3**, 346–350.
8 J. P. da Costa, P. S. Santos, A. C. Duarte and T. Rocha-Santos, *Science of The Total Environment*, 2016, **566**, 15–26.
9 A. Ter Halle, L. Jeanneau, M. Martignac, E. Jardé, B. Pedrono, L. Brach and J. Gigault, *Environmental Science & Technology*, 2017, **51**, 13689–13697.
10 K. Mattsson, E. V. Johnson, A. Malmendal, S. Linse, L.-A. Hansson and T. Cedervall, *Scientific Reports*, 2014, **7**, 11452.
11 R. Sussarellu, M. Suquet, Y. Thomas, C. Lambert, C. Fabioux, M. E. J. Pernet, N. Le Goïc, V. Quillien, C. Mingant, Y. Epelboin, C. Corporeau, J. Guyomarch, J. Robbens, I. Paul-Pont, P. Soudant and H. Arnaud, *Proceedings of the National Academy of Sciences*, 2016, **113**, 2430–2435.
12 M. Cole, P. Lindeque, C. Halsband and T. S. Galloway, *Marine Pollution Bulletin*, 2011, **62**, 2588–2597.
13 E. R. Zettler, T. J. Mincer and L. A. Amaral-Zettler, *Environmental Science & Technology*, 2013, **47**, 7137–7146.
14 L. Frere, L. Maignien, M. Chalopin, A. Huvet, E. Rinnert, H. Morrison, S. Kerninon, A.-L. Cassone, C. Lambert, J. Reveillaud and I. Paul-Pont, *Environmental Pollution*, 2018, **242**, 614e625.
15 V. Foulon, F. Le Roux, C. Lambert, A. Huvet, P. Soudant and I. Paul-Pont, *Environmental Science & Technology*, 2016, **50**, 10988–10996.
16 I. Kirstein, S. Kirmizi, A. Wichels, A. Garin-Fernandez, R. Erler, M. Löder and G. Gerdts, *Marine Environmental Research*, 2016, **120**, 1–8.
17 A. Andrady, *Marine Pollution Bulletin*, 2017, **119**, 12–22.
18 N. Lucas, C. Bienaime, C. Belloy, M. Queneudec, F. Silvestre and J.-E. Nava-Saucedo, *Chemosphere*, 2008, **73**, 429–442.
19 B. Laycock, M. Nikolic, J. M. Colwell, E. Gauthier, P. Halley, S. Bottle and G. George, *Progress in Polymer Science*, 2017, **71**, 144–189.
20 B. Alberts, A. Johnson, J. Lewis, D. Morgan, M. Rath, R. Keith and P. Walters, *Molecular biology of the cell*, Garland Science,

View Article Online
DOI: 10.1039/C9SM01482A

2014, vol. 1.

21 S. F. Nassar, A. Guinault, N. Delpouve, D. Veronique, V. Ducruet, C. Sollogoub and S. Domenek, *Polymer*, 2017, **108**, 163–172.

22 S. Schusser, S. Menzela, M. Backer, M. Leinhosa, Poghossiana, P. Wagner and M. Schoning, *Electrochimica Acta*, 2013, **113**, 779–784.

23 A. Kulkarni, J. Reiche, J. Hartmann, K. Kratz and L. A., *European Journal of Pharmaceutics and Biopharmaceutics*, 2008, **68**, 46–56.

24 M.-C. Morse, Q. Liao, C. S. Criddle and W. Frank, Curtis, *Polymer*, 2011, **52**, 547–556.

25 L. Suming, H. Garreau and M. Vert, *Journal of Materials Science: Materials in Medicine*, 1990, **1**, 198–206.

26 R. Auras, L.-T. Lim, S. E. Selke and H. Tsuji, *Poly(lactic acid): Synthesis, Structures, Properties, Processing, and Applications*, Wiley Series on Polymer Engineering and Technology, 2014, vol. 1.

27 H. Tsuji and S. Miyauchi, *Polymer degradation and stability*, 2001, **71**, 415–424.

28 S. Li and S. McCarthy, *Macromolecules*, 1999, **32**, 4454–4456.

29 Y. Kikkawa, H. Abe, T. Iwata, Y. Inoue and Y. Doi, *Biomacromolecules*, 2002, **3**, 350.

30 S. M. Hideto Tsuji, *Polymer*, 2001, **42**, 4463–4467.

31 D. F. Williams, *Eng. Med.*, 1981, **10**, 5–7.

32 H. Tsuji and S. Miyauchi, *Biomacromolecules*, 2001, **2**, 597.

33 M. S. Reeve, S. McCarthy, P. J. Milton, J. Downey and R. A. Gross, *Macromolecules*, 1994, **27**, 825.

34 R. T. MacDonald, S. P. McCarthy and R. A. Gross, *Macromolecules*, 1996, **29**, 7356–7361.

35 S. Li, A. Girard, H. Garreau and M. Vert, *Polymer Degradation and Stability*, 2000, **71**, 61–67.

36 D. C. Bassett, *Principles of Polymer Morphology, Cambridge Solid State Science Series, ISSN 0964-6752, Themes in the Social Sciences*, CUP Archive, 1981.

37 Y. Lin, K.-Y. Zhang, Z.-M. Dong, L.-S. Dong and Y.-S. Li, *Macromolecules*, 2007, **40**, 6257.

38 S. Wu, *Polymer interface and adhesion*, Taylor & Francis Group, 1983.

39 A. J. Barrett, J. F. Woessner and N. D. Rawlings, *Handbook of proteolytic enzymes*, Elsevier, 2012, vol. 1.

40 J. Bajorath, W. Hinrichs and W. Saenger, *The FEBS Journal*, 1988, **176**, 441–447.

41 O. Folin and V. Ciocalteau, *J Biol Chem*, 1929, **73**, 627–650.

42 J. Siepmann and A. Göpferich, *Adv Drug Deliv Rev*, 2001, **47**, 48:229.

43 F. von Burkersroda, L. Schedl and A. Göpferich, *Biomaterials*, 2001, **23**, 4221–4231.

44 H. Hopfenberg, *Controlled release from erodible slabs, cylinders, and spheres, in: D.R. Paul, F.W. Harris (Eds.), ACS Symp. Ser. No. 33.*, American Chemical Society, Washington, Controlled Release Polymeric Formulations, 1976.

45 D. Cooney, *AIChE J*, 1972, **18**, 446.

46 R. Abi-Akl, E. Ledieu, T. N. Enke, O. X. Cordero and T. Cohen, *Soft Matter*, 2019, **15**, 4098.

47 A. Göpferich and R. Langer, *Macromolecules*, 1993, **26**, 4105–4112.

48 K. Yamashita, Y. Kikkawa, K. Kurokawa and Y. Doi, *Biomacromolecules*, 2005, **6**, 850–857.

49 B. Crist and J. M. Schultz, *Progress in Polymer Science*, 2016, **56**, 1.

50 A. Ter Halle, L. Ladirat, X. Gendre, D. Goudouneche, C. Pusineri, C. Routaboul, C. Tenailleau, B. Duployer and E. Perez, *Environmental science & technology*, 2016, **50**, 5668–5675.

51 M. Salomez, M. George, P. Fabre, F. Touchaleaume, G. Cesar, A. Lajarrige and E. Gastaldi, *Polymer degradation and stability*, 2019, **167**, 102–113.